# *Comparative energy and exergy assessment of electrical- and thermal-compressor-assisted hybrid thermochemical cooling cycles*

***Doha Kafeh[a], Regis Olives[b], Driss Stitou[c] and Maxime Perier-Muzet[d]***

*[a] CNRS-PROMES UPVD, Perpignan, France, doha.kafeh@univ-perp.fr,*
*[b] CNRS-PROMES UPVD, Perpignan, France, olives@univ-perp.fr,*
*[c] CNRS-PROMES, Perpignan, France, driss.stitou@promes.cnrs.fr*
*[d] CNRS-PROMES UPVD, Perpignan, France, maxime.perier-muzet@univ-perp.fr, CA*

**Abstract:**

Hybridization of thermochemical refrigeration cycles with compression devices has emerged as an effective strategy to extend their operating range and enhance their applicability for low-temperature cooling. In this work, several hybrid thermochemical configurations assisted by either an electrical compressor or a thermally driven compressor are investigated. A steady-state thermodynamic model is developed to evaluate the performance of the $BaCl_2/NH_3$ reaction pair under different operating conditions, at an ambient temperature of $20\ °C$. The results confirm that hybridization significantly enlarges the operating domain of the cycle. In the non-assisted configuration, the minimum heat-source temperature required for decomposition is about $77\ °C$, while the lowest achievable cooling temperature is approximately $-4.3\ °C$. With assisted configurations, these limits can be lowered to about $41.7\ °C$ for the heat-source temperature and $-38.5\ °C$ for the cooling temperature. Electrical-compressor-assisted configurations provide the best compromise between operating range extension and thermodynamic performance, whereas thermal-compressor-assisted cycles exhibit larger performance degradation due to the additional heat required.

**Keywords:**

Thermochemical cooling; Hybrid sorption cycle; Electrical compressor; Thermal compressor; Exergy efficiency.

# 1. Introduction

Industrial processes reject a substantial amount of energy as waste heat, representing one of the largest untapped resources for improving energy efficiency and reducing carbon emissions. Recent reviews highlight that the vast majority of primary energy input in industrial sectors is ultimately lost as heat, particularly at low- to medium-temperature levels where direct reuse is challenging [1,2]. Although low-grade heat has limited thermodynamic potential, effective recovery and valorization strategies can significantly decrease fossil fuel consumption and associated $CO_2$ emissions, while contributing to industrial decarbonization pathways. At the same time, global cooling demand continues to rise, with conventional systems consuming up to 10% of total electricity worldwide, and even higher shares during peak periods in hot climates [3]. The widespread reliance on electricity-based vapor-compression systems thus contributes significantly to energy consumption and associated greenhouse gas emissions. In this context, thermally driven refrigeration technologies, which convert waste heat into useful cooling, offer a promising alternative to reduce both electricity demand and carbon footprint [1].

Among thermally driven cooling technologies, sorption-based systems, including absorption and thermochemical cycles, have received increasing attention for industrial waste heat recovery. Thermochemical cycles are particularly attractive because they rely on reversible solid–gas reactions and inherently provide thermal energy storage function. This capability allows these systems to adapt to fluctuating heat sources and cooling demands while offering high theoretical energy storage densities [2].

The development and deployment of sorption-based cooling systems have been limited by intrinsic thermodynamic constraints and economic factors. The operating conditions of these systems—pressure and temperature—are governed by two coupled thermodynamic equilibria (liquid–vapor and sorbent–sorbate), which strongly restrict their operational temperature range. To overcome these limitations, research efforts have focused on novel working pairs and advanced cycle architectures. Another approach involves integrating

auxiliary compression or expansion devices, such as compressors, expanders, or ejectors, into sorption systems [4,5]. Electrical-compressor-assisted thermochemical cycles have demonstrated extended operating ranges and improved functionality [6] ; however, electrical consumption remains a limiting factor, reducing the benefits of minimizing external energy dependency. In contrast, the potential of thermally driven compression devices, such as ejectors, to enhance the operating range of thermochemical cycles has received limited attention and remains largely unexplored.

To address this gap, the present study evaluates six hybrid thermochemical configurations based on the well know $BaCl_2/NH_3$ reactive pair. Two hybridization pathways are considered: electrical-compressor-assisted, as reported in previous studies, and a novel thermal-compressor-assisted configuration.

# 2. Cycle description

The thermochemical process is based on a reversible solid–gas reaction occurring in a thermochemical reactor, which can be expressed as:

$$S_0 + \nu.G \rightleftharpoons S_1 + \nu.\Delta_r H^0 \quad (1)$$

The forward reaction corresponds to the synthesis phase, in which the desorbed salt ($S_0$) reacts with $\nu$ moles of gas to form ($S_1$) , releasing heat equal to the standard reaction enthalpy ($\Delta_r H^0$). The reverse reaction represents the decomposition phase, which is endothermic. The reaction is monovariant, with temperature and pressure linked through the Clausius–Clapeyron equation:

$$P_{eq} = P_0.\exp\left(\frac{-\Delta_r H^0}{R.T} + \frac{\Delta_r S^0}{R}\right) \quad (2)$$

where $P_{eq}$ is the equilibrium pressure at temperature $T$, and $\Delta_r H°$ and $\Delta_r S°$ are the standard reaction enthalpy and entropy, respectively, under standard conditions ($P_0 = 1bar\,; T_0 = 25°C$) .
In addition to the reactor, a basic thermochemical process includes an evaporator, a condenser, and an ammonia storage tank. The process operates in two active phases: charging (endothermal reaction of decomposition) and discharging (exothermal reaction of synthesis) separated by a standby phase (storage). Depending on the operating conditions, the thermochemical cycle can operate either in a non-assisted mode or in a hybrid mode assisted by an electrical or a thermal compressor**.**

## 2.1. Operating of a basic thermochemical system

During the non-assisted charging phase, the active components are the reactor and condenser (Fig 1). Initially, the reactor is disconnected from the condenser and is heated by the hot source, available at $T_{dec}$. As the reactor temperature rises, the internal pressure increases, inducing thermal compression. When the reactor pressure exceeds the condenser saturation pressure ($P_{cond} = P_{sat,NH_3}(T_{cond})$), the reactor and condenser are connected. At this stage, the reactor pressure equilibrates with the condenser pressure ($P_{dec} = P_{cond}$), while the reactor temperature remains above the equilibrium temperature of the solid–gas reaction ($T_{dec} > T_{dec}^{eq}(P_{cond})$). Under these conditions, the endothermic decomposition reaction occurs in the reactor. The released ammonia vapor $(1 \rightarrow 2)$ condenses in the condenser, rejecting heat $Q_{cond}$ to the ambient, and is subsequently transferred in liquid form to the storage tank at ambient temperature $(2 \rightarrow 3)$. The charging phase continues until the heat input stops, or the reactive material is fully decomposed. Afterward, the reactor is disconnected, and the system enters the standby storage stage.

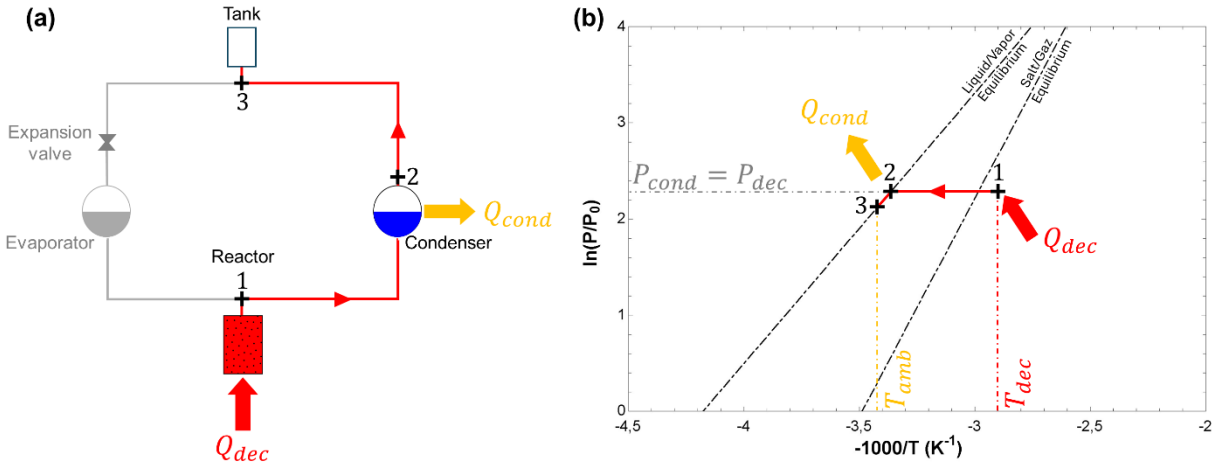


***Figure. 1.*** *Schematic of the non-assisted decomposition phase (a) and corresponding Clausius–Clapeyron representation (b)*

During the non-assisted discharging phase, the active components are the reactor and the evaporator (Fig 2). The process starts with reactor cooling through heat exchange with the ambient sink at $T_{amb}$. When the reactor pressure falls below that of the evaporator, the two components are reconnected. At this point, the reactor pressure equilibrates with that of the evaporator $(P_{ev} = P_{syn})$, while the reactor temperature decreases below the equilibrium temperature of the solid–gas reaction $(T_{syn} < T_{syn}^{eq})$. Meanwhile, the liquid stored in the reservoir at ambient temperature $(T_{amb})$ passes through an expansion valve, reducing its pressure to the evaporation level $(3 \rightarrow 4)$. Under these conditions, liquid evaporation begins in the evaporator $(4 \rightarrow 5)$. The vapor produced then flows into the reactor $(5 \rightarrow 6)$ where the exothermic synthesis reaction takes place, releasing the reaction heat $(Q_{syn})$. This evaporation process is endothermic and absorbs heat from the cold source, thereby generating the desired cooling effect $(Q_{cold})$.

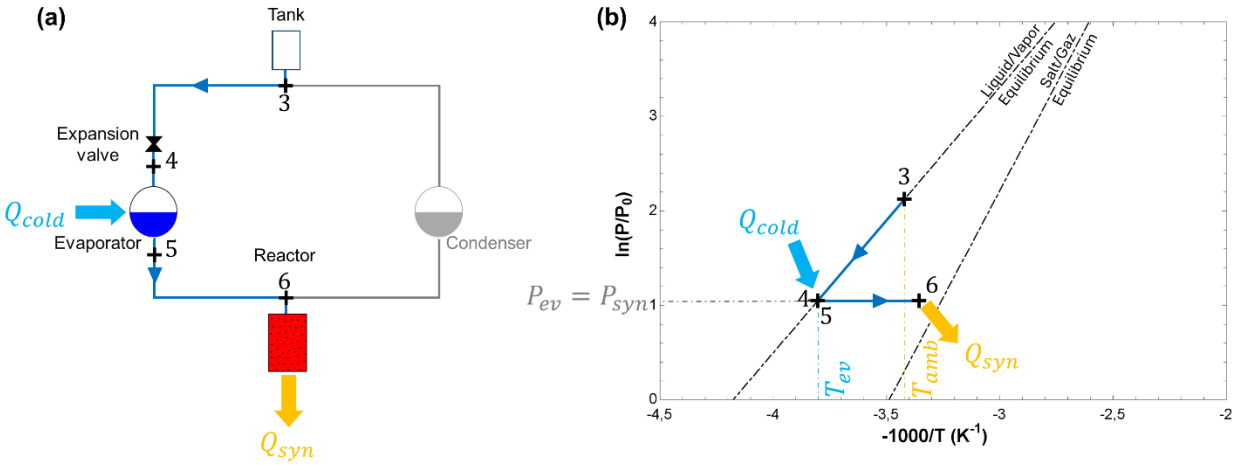


***Figure. 2.*** *Schematic of the non-assisted synthesis phase (a) and corresponding Clausius–Clapeyron representation (b)*

## 2.2. Hybridization strategies

To extend the operating range of the thermochemical cycle, assisted configurations are considered. Hybridization can be applied during the decomposition phase, the synthesis phase, or both. Two types of assistance are investigated: electrical compression and thermal compression. The corresponding operating principles are described in the following sections.

### 2.2.1. Electrical-compressor-assisted configurations

When the heat source temperature is insufficient to drive decomposition at the condenser pressure $(P_{dec} < P_{cond})$, an electrical compressor introduced between the reactor and the condenser (Fig 3) is then

required. The ammonia vapor released from the reactor is first compressed $(1 \rightarrow 2)$ and then directed to the condenser $(2 \rightarrow 3)$, where it condenses and rejects the latent heat $Q_{cond}$ to the ambient sink. The condensed liquid is subsequently stored in the reservoir for later use $(3 \rightarrow 4)$.

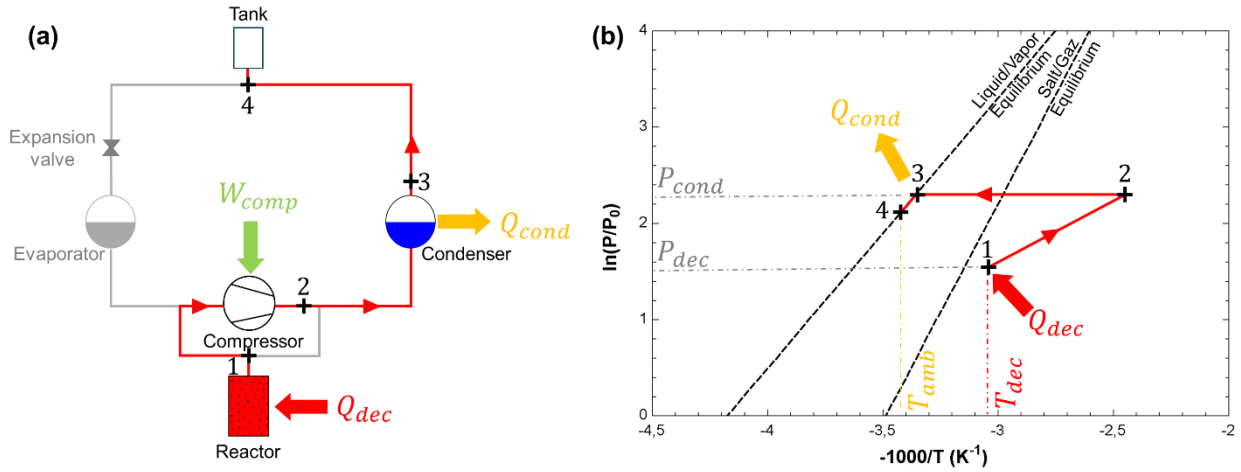


***Figure. 3.*** *Schematic of electrical-compressor-assisted decomposition (a) and corresponding representation on the Clausius–Clapeyron diagram (b)*

When lower cooling temperatures are required, the evaporator pressure corresponding to the cold production temperature may become lower than the reactor pressure at the synthesis temperature $(P_{ev} < P_{syn})$. Under these conditions, vapor cannot naturally flow from the evaporator to the reactor, preventing the synthesis reaction to proceed. To overcome this limitation, an electrical compressor is implemented between the evaporator and the reactor (Fig 4). The process begins with the expansion of the liquid ammonia to the evaporation pressure $(4 \rightarrow 5)$. The resulting evaporation in the evaporator $(5 \rightarrow 6)$ produces the cooling effect $Q_{cold}$. The generated vapor is then compressed $(6 \rightarrow 7)$ and directed toward the reactor, where the exothermic synthesis reaction occurs, releasing the reaction heat $(7 \rightarrow 8)$.

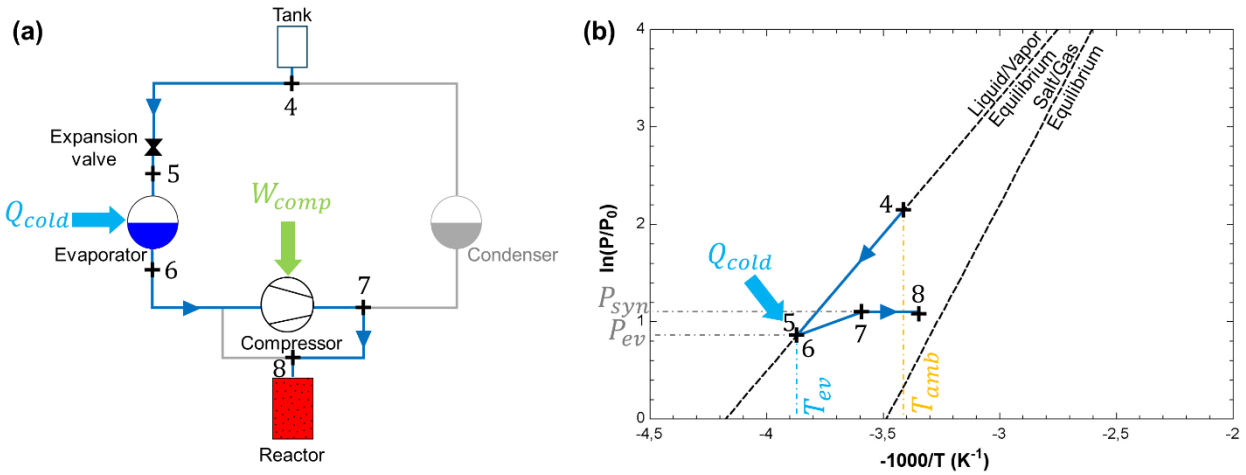


***Figure. 4.*** *Schematic of electrical-compressor-assisted synthesis (a) and corresponding representation on the Clausius–Clapeyron diagram (b)*

## 2.2.2. Thermal-compressor-assisted configurations

In this work, the thermal compressor represents thermally driven compression devices such as ejecto-compressors or turbocompressors. When the heat source temperature is insufficient to drive the decomposition phase at the condenser pressure, a thermal compressor is introduced between the reactor and the condenser (Fig 5). The device operates according to an ejector-like principle, where a high-pressure primary flow expands to entrain and compress a low-pressure secondary flow. In the proposed configuration, the driving energy is provided by thermal input $Q_{VG}$ supplied to a vapor generator. The vapor produced in the generator $(4 \rightarrow 5)$ acts as the primary flow and expands through the expander $(5 \rightarrow 5')$, generating the work

required to compress the secondary vapor leaving the reactor $(1 \rightarrow 1')$. The two streams are then mixed $(2)$ and directed toward the condenser $(2 \rightarrow 3)$, where condensation occurs and the latent heat $Q_{cond}$ is rejected to the ambient environment. The condensed liquid is subsequently split into two streams: one part is stored in the reservoir at ambient temperature for later use $(3 \rightarrow 6)$, while the other is pumped $(3 \rightarrow 4)$ back to the vapor generator, where it is vaporized again.

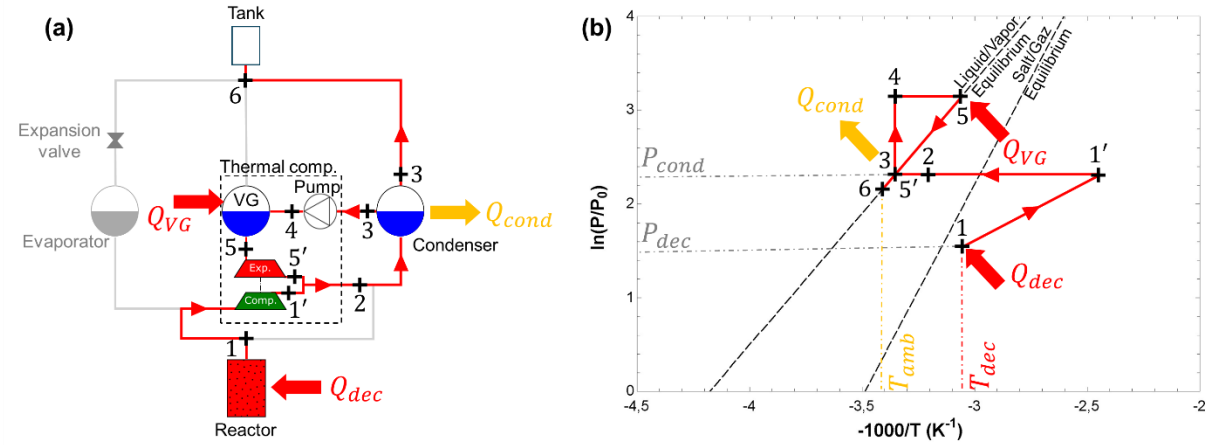


***Figure. 5.*** *Schematic of thermal-compressor-assisted decomposition (a) and corresponding representation on the Clausius–Clapeyron diagram (b)*

Similarly to the electrically assisted synthesis configuration, when the evaporator requires a lower pressure than the reactor pressure for a deeper cold production, the synthesis reaction cannot proceed. To overcome this limitation, a thermal compressor is installed between the evaporator and the reactor to enable vapor transfer (Fig 6). In this configuration, the process begins by expanding the liquid ammonia to the evaporation pressure $(6 \rightarrow 7)$. The vapor generated in the evaporator $(7 \rightarrow 8)$, referred to as the secondary flow, is then entrained and compressed by the thermal compressor $(8 \rightarrow 8')$. The compression process is driven by a high-pressure primary flow, produced by vaporizing part of the working fluid stored in the reservoir using a fraction of the heat released during the synthesis reaction $(6 \rightarrow 9)$.This high-pressure vapor expands through the expansion stage of the thermal compressor $(9 \rightarrow 9')$, providing the work required to entrain and compress the secondary flow. The two streams subsequently mix $(10)$ and the resulting flow is directed toward the reactor, where the exothermic synthesis reaction occurs $(10 \rightarrow 11)$.

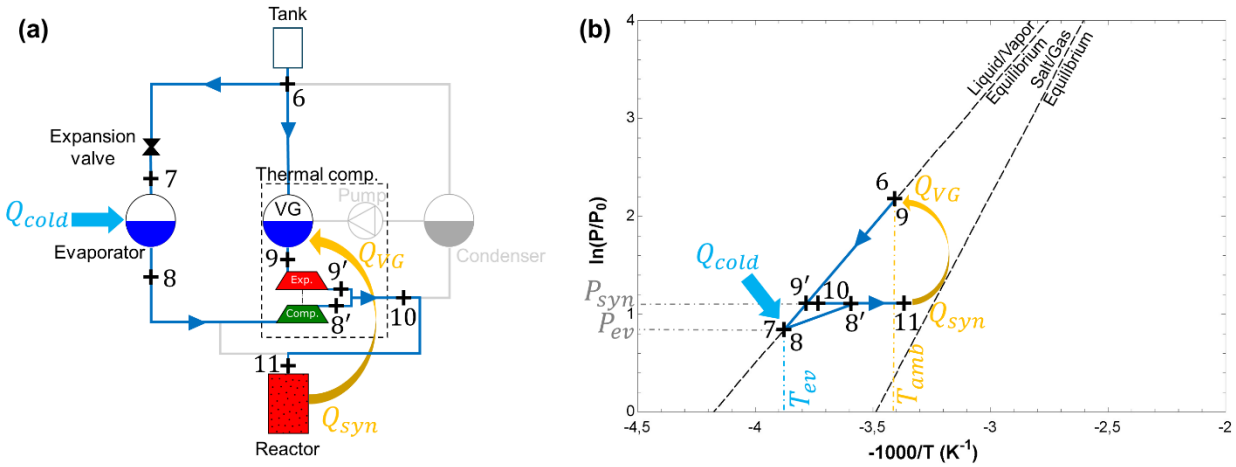


***Figure. 6.*** *Schematic of thermal-compressor-assisted synthesis (a) and corresponding representation on the Clausius–Clapeyron diagram (b)*

# 3. Thermodynamic modeling

The thermodynamic model used in this study is based on a zero-dimensional steady-state (0D) approach inspired by Godefroy et al. [5], combining mass and energy balances with phase-equilibrium relations applied to each component of the system.

The main modeling assumptions are as follows:

- The cycle operates in steady state.
- The reactor, evaporator, condenser and vapor generator exchange heat only with their respective sources or sinks, with a temperature pinch $\Delta T_{pinc}$ .
- The ammonia is saturated liquid and vapour at the outlet of the condenser and the evaporator respectively.
- Pressure drops are neglected.
- For the thermochemical reactor, a temperature deviation from thermodynamic equilibrium $\Delta T_{eq}$ is imposed to drive the reaction.
- The pump, electrical compressor, and thermal compressor operate with fixed isentropic efficiencies.
- A maximum compression ratio $\tau_{comp}^{max}$ is considered for both compressors.
- The expansion valve is ideal and modeled as an isenthalpic throttling device.
- The ambient temperature is taken as the thermodynamic reference state $(T_0 = T_{amb})$ for all exergy calculations.
- A maximum reaction advancement range $\Delta X$ and a maximum pressure $P_{max}$ at the vapor generator outlet are imposed.

In the non-assisted cycle, the reactor pressure during decomposition is imposed by the condenser pressure, allowing the required hot-source temperature to be determined while accounting for the equilibrium deviation. During synthesis, the reactor temperature is defined relative to the ambient temperature with a minimum temperature difference, while the pressure corresponds to the evaporator pressure. In contrast, in the assisted configurations, the reactor pressure is no longer constrained by the condenser or evaporator. The operating conditions are directly determined from the hot-source and ambient temperatures using the equilibrium relation Eq. (2) The reactor states during decomposition and synthesis are therefore expressed as:

$$T_{dec} = T_{hot} - \Delta T_{pinc} \text{ and } P_{dec} = P_0 . \exp\left(\frac{-\Delta_r H^0}{R.\left(T_{dec} - \Delta T_{eq}\right)} + \frac{\Delta_r S^0}{R}\right) \quad (3)$$

$$T_{syn} = T_{amb} + \Delta T_{pinc} \text{ and } P_{syn} = P_0 . \exp\left(\frac{-\Delta_r H^0}{R.\left(T_{syn} + \Delta T_{eq}\right)} + \frac{\Delta_r S^0}{R}\right) \quad (4)$$

For the auxiliary components, the condenser and evaporator deliver saturated streams at their outlets. Their operating conditions are defined by the ambient sink or the cold source, and the temperature pinch, as given by:

$$T_{cond} = T_{amb} + \Delta T_{pinc} \text{ and } P_{cond} = P_{sat}(T_{cond}) \quad (5)$$

$$T_{ev} = T_{cold} - \Delta T_{pinc} \text{ and } P_{ev} = P_{sat}(T_{ev}) \quad (6)$$

For the thermal-compressor-assisted configurations, the vapor generator (VG) produces saturated vapor with a minimum temperature difference relative to its heat source:

$$T_{VG} = T_{syn} - \Delta T_{pinc} \quad \text{or} \quad T_{VG} = T_{hot} - \Delta T_{pinc} \quad \text{and } P_{VG} = P_{sat}(T_{VG}) \quad (7)$$

Once the equilibrium states are determined, thermodynamic properties (enthalpy and entropy) are evaluated using the ammonia property correlations available in EES. The thermal compressor is modeled as a coupled compressor–expander system connected at a mixing junction. The expander is driven by high-pressure vapor supplied by the vapor generator. The device operates adiabatically, and the work produced by the expander is assumed to drive the compression process. By applying the first law of thermodynamics, the relationship between the expansion and compression works is: $(W_{exp} = |W_{comp}|)$. The primary (expanded) and secondary (compressed) ammonia streams are mixed at a junction (b). To determine the thermodynamic state of the mixture at the thermal compressor outlet, material and energy balances are

applied:

$$n_s + n_p - n_b = 0 \tag{8}$$

$$n_s h_s^{in} + n_p h_p^{in} - n_b h_b = 0 \tag{9}$$

These equations relate the mass flow rates and the specific enthalpies of the primary and secondary streams to those of the mixture. The determination of the required amount of primary ammonia to entrain a given secondary ammonia flow is then based on the energy analysis of each flow.

For the compressed flow (secondary flow):

$$W_{comp}^{th} + n_s.(h_s^{in} - h_s^{out}) = 0 \quad \text{with} \quad \eta_{comp}^{is,th} = \frac{h_s^{out,is} - h_s^{in}}{h_s^{out} - h_s^{in}} \tag{10}$$

Similarly, for the expanded flow (primary flow):

$$W_{exp} + n_p.\left(h_p^{in} - h_p^{out}\right) = 0 \quad \text{with} \quad \eta_{exp}^{is} = \frac{h_p^{out} - h_p^{in}}{h_p^{out,is} - h_p^{in}} \tag{11}$$

Once the cycle trajectory is established, the system performance is evaluated using the coefficient of performance (COP) and the exergy efficiency.

$$COP = \frac{Q_{cold}}{Q_{in}} \tag{12}$$

where $Q_{cold}$ is the cooling capacity produced in the evaporator, and $Q_{in}$ is the total external energy supplied to the system. The exchanged masses and energies are determined from mass and energy balances over all components of the system.
For the thermal-compressor-assisted decomposition configurations, the total external energy input includes the heat supplied to the reactor during decomposition, the heat supplied to the vapor generator, and the pump work ($Q_{in} = Q_{dec} + Q_{VG} + W_{pump}$).
For the thermal-compressor-assisted synthesis configuration, the vapor generator is supplied by the heat released during the synthesis reaction. Since this heat corresponds to an internal energy transfer, it is not considered as external input. The external energy input therefore becomes: ($Q_{in} = Q_{dec}$).
For the electrical-compressor-assisted configurations, the external energy input includes the heat supplied to the reactor and the electrical work consumed by the compressor ($Q_{in} = Q_{dec} + W_{comp}$).
The exergy efficiency is expressed as:

$$\eta_{ex} = \frac{|\, Ex_{cold} \,|}{Ex_{in}} \tag{13}$$

with

$$Ex_{cold} = Q_{cold}.\left(1 - \frac{T_{amb}}{T_{cold}}\right) \tag{14}$$

and

$$Ex_{in} = (Q_{dec} + Q_{GV}).\left(1 - \frac{T_{amb}}{T_{hot}}\right) + W_{pump} \quad or \quad Ex_{in} = Q_{dec}.\left(1 - \frac{T_{amb}}{T_{hot}}\right) + W_{comp} \tag{15}$$

# 4. Results and discussion

## 4.1. Case study and operating conditions

The thermodynamic analysis is performed under the following nominal operating conditions: a cooling capacity of $Q_{cold} = 1$ kWh and an ambient temperature of $T_{amb} = 20$°C. The thermochemical pair considered in this study is barium chloride–ammonia, described by the reaction:

$$BaCl_2 + 8.NH_3 \rightleftharpoons BaCl_2(NH_3)_8 + 8.\Delta_r H° \tag{16}$$

Barium chloride is widely used in thermochemical refrigeration systems due to its favourable reaction enthalpy and compatibility with ammonia, particularly for low-temperature refrigeration and deep-freezing applications.

The main design and operating parameters used in the simulations are summarized in Table 1.

***Table 1.*** *Operating and design parameters considered for the thermodynamic simulations.*

| | | |
|---|---|---|
| Heat exchange temperature pinch | | $\Delta T_{pinc} = 5\ K$ |
| Deviation from the equilibrium temperature in the reactor | Non-assisted mode | $10\ K\ \leq \Delta T_{eq}\ \leq 100\ K$ |
| | Assisted mode | $\Delta T_{eq} = 10\ K$ |
| Isentropic efficiency of the | Pump | $\eta_{pump}^{is} = 0.6$ |
| | Thermal compressor (compression and expansion stages) | $\eta_{comp}^{is,th} = \eta_{exp}^{is} = 0.7$ |
| | Electrical compressor | $\eta_{comp}^{is,ele} = 0.7$ |
| Maximum compression ratio of ejector compressed flow | | $\tau_{max} = 5$ |
| Maximum reaction advancement rang | | $\Delta X = 0{,}8$ |

## 4.2. Mollier diagrams

The Mollier diagram (pressure–enthalpy) shown in Fig 7 illustrates the thermodynamic trajectory of the ammonia working fluid for the hybrid thermochemical cycles. The saturation curve of pure ammonia is represented by the bold black line, while the thin red curves correspond to isotherms. On the $P$–$h$ diagram, the hybrid cycle is represented by bold red lines for the decomposition phase and bold blue lines for the synthesis phase.

For the dual electrical-compressor-assisted configuration (Fig 7 (a)), ammonia leaving the reactor is compressed from $P_{dec} = 474$ kPa, corresponding to a heat-source temperature $T_{hot} = 60$°C, to the condenser pressure $P_{cond} = 998.2$ kPa using the electrical compressor. In the absence of compression assistance and for an equilibrium deviation of 10 K, a higher heat-source temperature of approximately 77°C would be required to reach this pressure level.

After compression, the ammonia vapor is directed to the condenser, where it is liquefied and stored in the reservoir $(2 \rightarrow 4)$. During the cooling production phase, the liquid ammonia undergoes an isenthalpic expansion $(4 \rightarrow 5)$, followed by evaporation in the evaporator $(5 \rightarrow 6)$ at $P_{ev} = 234$ kPa, corresponding to a cooling temperature $T_{cold} = -10$°C. However, the reactor synthesis pressure is $P_{syn} = 289.9$ kPa, which would correspond to a minimum evaporation temperature of approximately $-4.3$°C for an equilibrium deviation of $10\ K$. To overcome this pressure gap, the vapor produced in the evaporator is compressed $(6 \rightarrow 7)$before entering the reactor $(7 \rightarrow 8)$, where the exothermic synthesis reaction takes place.

In the thermal-compressor-assisted configuration (Fig 7 (b)), compression is achieved using a thermally driven motive flow. This primary flow is first pumped from the liquid reservoir $(3 \rightarrow 4)$and vaporized in the vapor generator $(4 \rightarrow 5)$. The expansion of this motive flow $(5 \rightarrow 5')$provides the mechanical energy required to compress the low-pressure vapor leaving the reactor. The two streams are then mixed at state 2, and the mixture is directed toward the condenser, where it is liquefied and stored $(2 \rightarrow 6)$.

A similar mechanism is applied during the synthesis phase. The vapor leaving the evaporator $(8 \rightarrow 8')$ is compressed through the expansion of the primary flow. In this case, the heat required to generate the motive flow is supplied by the exothermic heat released during the synthesis reaction, enabling compression without external electrical energy input.

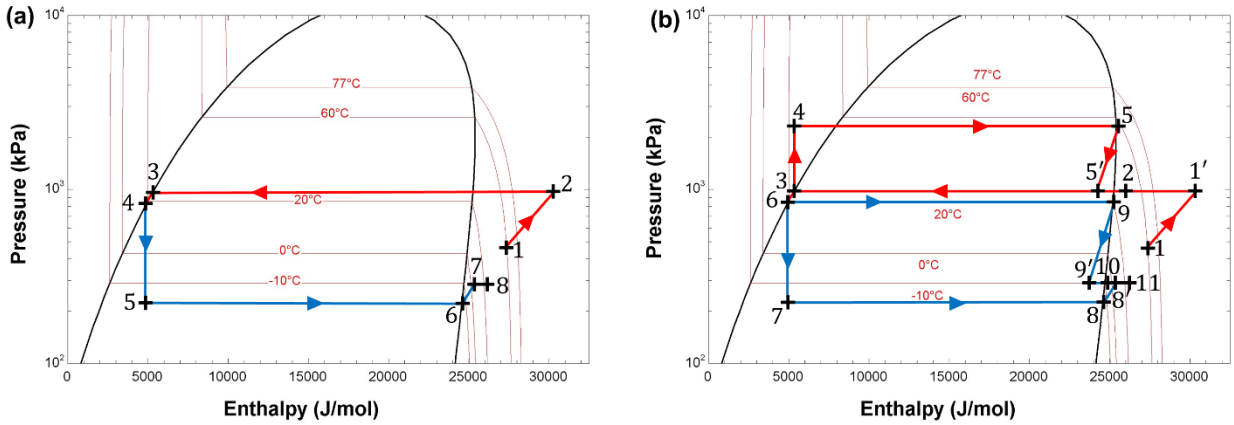


***Figure. 7.*** *Mollier diagrams of the dual electrical-compressor-assisted thermochemical cycle (a) and the thermal-compressor-assisted thermochemical cycle (b).*

## 4.3. Extension of the operating range

The thermodynamic model allows the operating range of the thermochemical cycle to be evaluated as a function of the hot-source temperature $T_{hot}$ and the cold-production temperature $T_{cold}$. Figure 8 presents the evolution of the coefficient of performance (COP) within this operating domain. In the non-assisted configuration, the limits of operation are mainly imposed by the equilibrium conditions of the thermochemical reaction and by the pressure levels imposed by the condenser and evaporator. During decomposition, the minimum hot-source temperature required to reach the condenser pressure $P_{cond} = 998.2$ kPa is approximately $77$°C. During synthesis, the reactor equilibrium pressure reaches $289.9$ kPa, corresponding to a minimum evaporation temperature of about $-4.3$°C. Hybridization significantly extends these limits: decomposition-assisted operation reduces the minimum hot-source temperature to approximately $41.7$°C, while synthesis-assisted operation enables cooling production down to about $-38.5$°C.

Although hybridization enlarges the feasible operating domain, it also leads to a decrease in COP. This effect is illustrated by the isothermal sections in Fig. 10. For a fixed heat-source temperature $T_{hot} = 120$°C (Fig 10 (a)), the COP decreases as $T_{cold}$ decreases because a larger amount of ammonia must be evaporated to produce the same cooling capacity at lower temperatures, increasing the thermal energy required for decomposition. When electrical compression assistance is introduced, the COP decreases more rapidly due to the additional electrical work required as the compression ratio increases with decreasing evaporation pressure. The decrease becomes even more pronounced for the thermal-compressor-assisted configuration, where the reduction in COP results not only from the higher ammonia flow rate but also from the additional primary vapor required in the vapor generator to entrain the secondary flow. As the operating limits are approached, the heat demand in the vapor generator increases significantly, which may lead to COP values below 0.1. A second isothermal section (Fig. 10 (b)) obtained for $T_{cold} = -10$°C shows that in the non-assisted configuration the COP decreases as $T_{hot}$increases, mainly due to the additional sensible heat required to heat the reactor. In the assisted configurations, the electrical-compressor-assisted cycle is mainly affected by the increase in compressor work as the compression ratio rises when $T_{hot}$ decreases, whereas the thermal-compressor-assisted configuration shows a stronger degradation because the amount of primary vapor required to drive the thermal compressor increases significantly at low temperatures.

Figure 9 presents the variation of the exergy efficiency $\eta_{ex}$ for the $BaCl_2$ $(8/0)$ cycle. Unlike the COP, the exergy efficiency does not necessarily decrease with hybridization, and in several regions assisted configurations even exhibit higher values than the non-assisted cycle. In the non-assisted configuration, $\eta_{ex}$ increases as the evaporation temperature decreases due to the increase of the Carnot factor, which raises the useful exergy associated with the cooling effect. With electrical compression assistance, the system can operate at lower evaporation temperatures while maintaining relatively high exergy efficiency; for example, at $T_{hot} = 120$°C (Fig 10 (a)), $\eta_{ex}$ continues to increase beyond the non-assisted limit of $-4.3$°C, indicating that the gain in useful cooling exergy compensates for the additional compressor work. In contrast, for the thermal-compressor-assisted synthesis configuration, $\eta_{ex}$gradually decreases as $T_{cold}$ decreases because larger amounts of primary vapor must be generated in the vapor generator, increasing the exergy input. This difference is also observed in decomposition-assisted operation (Fig 10 (b)), where the electrical-compressor-assisted configuration consistently achieves higher exergy efficiency than the thermal-compressor-assisted

configuration. Overall, hybridization extends the operating range toward lower heat source and cooling temperatures, but this flexibility is obtained at the cost of additional energy consumption associated with compression processes. Among the investigated options, synthesis-assisted operation with an electrical compressor provides the most favorable compromise between operating flexibility and thermodynamic performance.

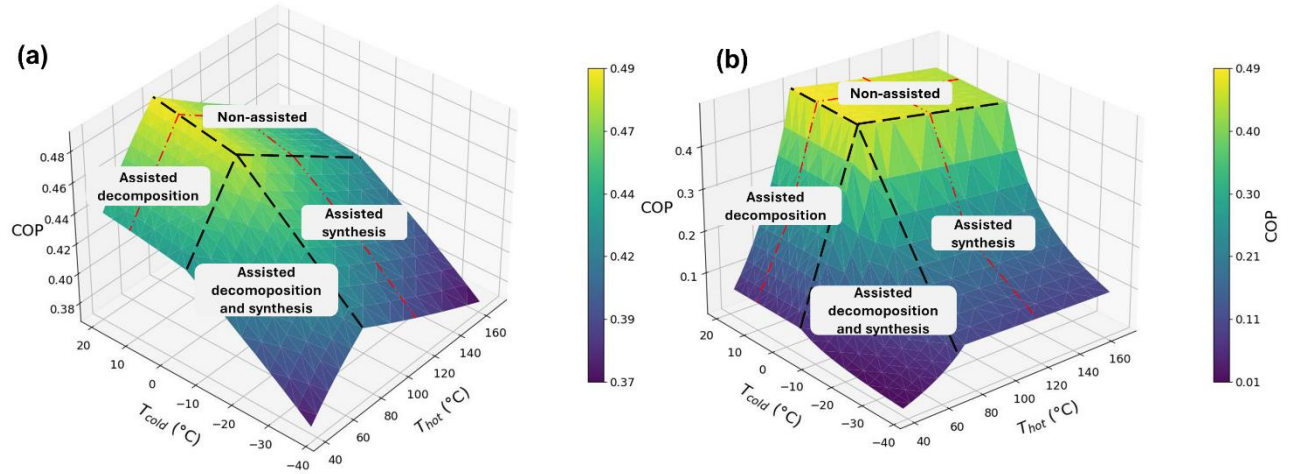


***Figure. 8.*** *COP maps as a function of hot-source and cold-sink temperatures for electrical- compressor-assisted (a) and thermal-compressor-assisted (b) thermochemical cycles.*

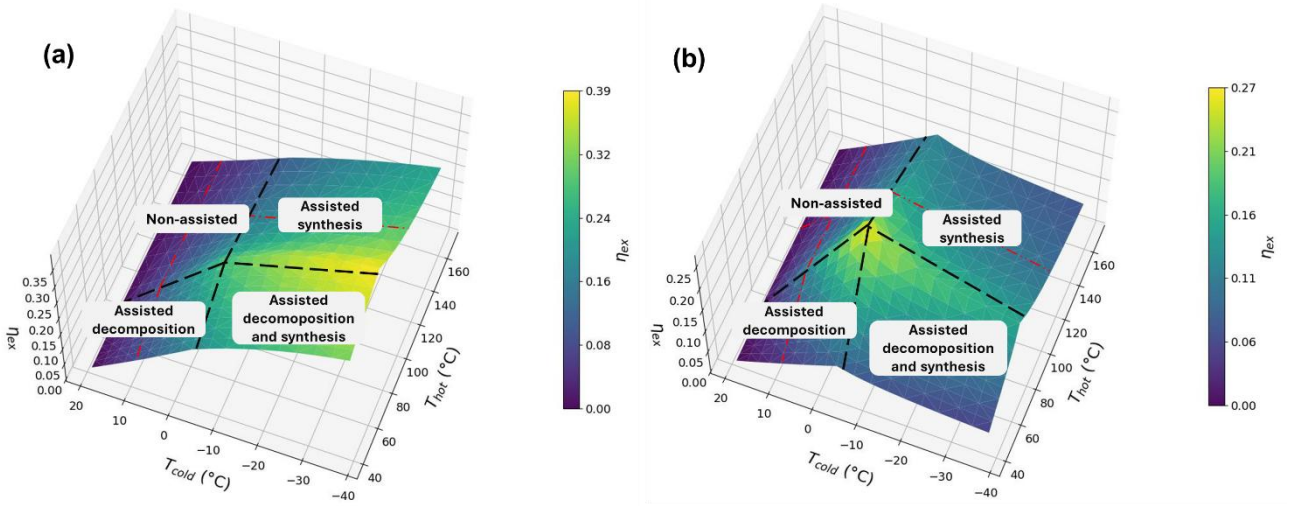


***Figure. 9.*** *Exergy efficiency maps as a function of hot-source and cold-sink temperatures for electrical-compressor-assisted (a) and thermal-compressor-assisted (b) thermochemical cycles.*

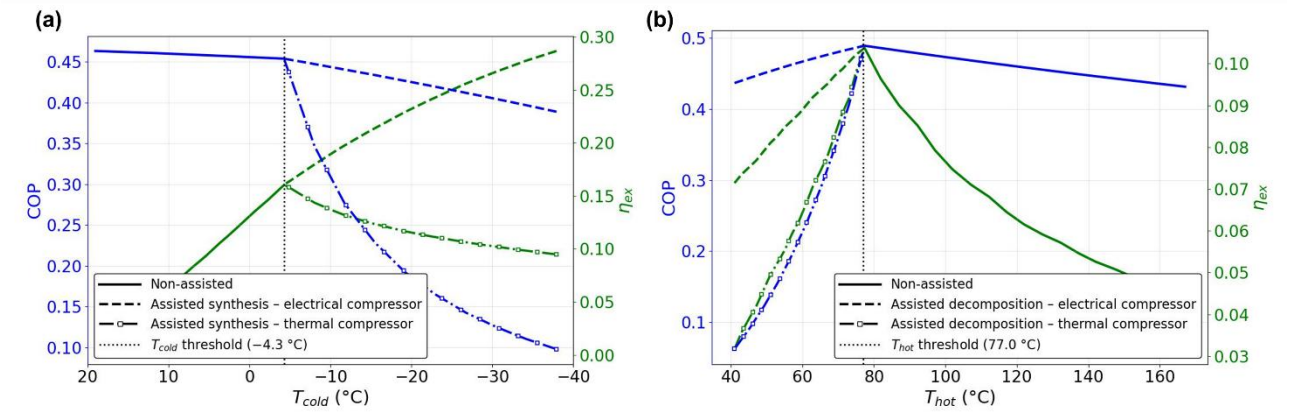


***Figure. 10.*** *Evolution of the coefficient of performance (COP) and exergy efficiency for the different operating configurations. (a): variation with the cold-source temperature for a fixed $T_{hot} = 120°C$. (b): variation with the hot-source temperature for a fixed $T_{cold} = -10°C$.*

# 4. Conclusion

This work investigated the potential of hybrid thermochemical refrigeration cycles to extend the operating range of conventional solid–gas thermochemical systems. A zero-dimensional steady-state thermodynamic model was developed to analyze several configurations based on the $BaCl_2/NH_3$ reaction pair, including non-assisted cycles and hybrid configurations assisted by either electrical or thermal compression.

The results confirm that hybridization significantly extends the operating limits of thermochemical refrigeration systems. In the non-assisted configuration, the operating range is mainly constrained by the thermodynamic equilibrium of the reactor and by the pressure levels imposed by the condenser and evaporator. For the studied case, the minimum hot-source temperature required for decomposition is approximately $77\,°C$, while the minimum achievable cooling temperature is about $-4.3\,°C$. By introducing assisted configurations, these limits can be substantially extended and lowered: the hot-source temperature can be reduced to approximately $41.7\,°C$ in decomposition-assisted mode, while synthesis-assisted operation enables cooling production down to about $-38.5\,°C$. However, this extension of the operating range is associated with a decrease in the coefficient of performance (COP), whereas the evolution of exergy efficiency depends on the hybridization strategy and the operating conditions. Synthesis-assisted configurations with an electrical compressor can maintain relatively high and stable exergy efficiency over the wide extended range of cold-production temperatures. In contrast, thermal-compressor-assisted configurations exhibit a stronger degradation of performance near the operating limits due to the additional heat required to generate the primary vapor in the vapor generator. Overall, the results highlight the trade-off between operating flexibility and thermodynamic efficiency. Hybrid thermochemical cycles therefore represent a promising pathway for the valorization of low-grade heat while enabling refrigeration at temperatures lower than those achievable with conventional thermochemical systems.

Future work will focus on the experimental validation of the thermal compression hybrid configurations in order to confirm the thermodynamic predictions of the model. In particular, the integration of micro-ejector-based thermal compressors will be investigated as a compact and passive solution for thermally driven compression. Additional studies will also explore alternative cycle architectures and other reactive salts to further improve both the operating range and the overall system performance.

# Acknowledgments

Doha Kafeh receives a PhD grant from the Ministry of Education (doctoral contract n° 2024-09-ED.305, UPVD, Perpignan, France).

# Nomenclature

**Variables**

| | |
|---|---|
| $c_p$ | molar heat capacity, J/(mol K) |
| $Ex$ | exergy, J |
| $h$ | molar specific enthalpy, J/mol |
| $n$ | number of moles, mol |
| $P$ | pressure, Pa |
| $Q$ | heat, J |
| $R$ | ideal gas constant, J/(mol K) |
| $s$ | molar specific entropy, J/(mol K) |
| $T$ | temperature, °C |
| $W$ | mechanical work, J |
| $X$ | reaction extent |

**Greek symbols**

| | |
|---|---|
| $\eta$ | efficiency |
| $\Delta_r H^0$ | standard enthalpy of reaction |
| $\Delta_r s^0$ | standard entropy of reaction |
| $\Delta X$ | reaction advancement range |

**Subscripts and superscripts**

| | |
|---|---|
| $amb$ | ambient |
| $an$ | anhydrous salt |
| $cold$ | cold source |
| $comp$ | compression |
| $cond$ | condenser |
| $dec$ | decomposition |
| $eq$ | equilibrium |
| $ev$ | evaporator |
| $ex$ | exergetic |
| $exp$ | expansion |
| $hot$ | hot source |
| $in$ | input |
| $is$ | isentropic |
| $max$ | maximum |
| $out$ | output |
| $p$ | primary flow |
| $pinc$ | pinc point |

| | | | |
|---|---|---|---|
| $s$ | secondary flow | ° | standard conditions |
| $sat$ | saturation | $VG$ | vapor generator |
| $syn$ | synthesis | $Th$ | thermal |

# References


[1] Ji D., Liu G., Romagnoli A., Rajoo S., Besagni G., Markides CN., Low-grade thermal energy utilization: Technologies and applications. Applied Thermal Engineering 2024; 244:122618.

[2] Rahbari HR., Elmegaard B., Bellos E., Tzivanidis C., Arabkoohsar A., Thermochemical technologies for industrial waste heat recovery: A comprehensive review. Renewable and Sustainable Energy Reviews 2025; 215:115598.

[3] Howarth N., Camarasa C., Lane K., Risquez Martin A., Keeping cool in a hotter world is using more energy, making efficiency more important than ever. Paris, France: International Energy Agency (IEA); 2023.

[4] Ferrucci F., Stitou D., Ortega P., Lucas F., Mechanical compressor-driven thermochemical storage for cooling applications in tropical insular regions. Energy Procedia 2017; 142:3415–20.

[5] Godefroy A., Perier-Muzet M., Neveu P., Mazet N., Hybrid thermochemical cycles for low-grade heat storage and conversion into cold and/or power. Energy Conversion and Management 2020; 225:113347.

[6] Perrigot A., Perier-Muzet M., Ortega P., Stitou D., Thermodynamic performance's analysis of a cold production by hybrid compressor-based thermochemical sorption processes using ammoniated salts. Energy Conversion and Management 2022; 267:115931.